

## Magnetohydrodynamics with Implicit Plasma Simulation

J. U. Brackbill<sup>1,\*</sup> and G. Lapenta<sup>2</sup>

<sup>1</sup> *Los Alamos National Laboratory (retired), Los Alamos, NM 87544, USA.*

<sup>2</sup> *Centrum voor Plasma-Astrofysica, Departement Wiskunde, Katholieke Universiteit Leuven, Celestijnenlaan 200B, 3001 Leuven, Belgium.*

Received 21 November 2007; Accepted (in revised version) 8 January 2008

Available online 14 April 2008

---

**Abstract.** We consider whether implicit simulation techniques can be extended in time and space scales to magnetohydrodynamics without any change but the addition of collisions. Our goal is to couple fluid and kinetic models together for application to multi-scale problems. Within a simulation framework, transition from one model to the other would occur not by a change of algorithm, but by a change of parameters. This would greatly simplify the coupling. Along the way, we have found new ways to impose consistent boundary conditions for the field solver that result in charge and energy conservation, and establish that numerically-generated stochastic heating is the problem to overcome. For an MHD-like problem, collisions are clearly necessary to reduce the stochastic heating. Without collisions, the heating rate is unacceptable. With collisions, the heating rate is significantly reduced.

**PACS:** 52.65.-y, 52.65Rr, 52.65Kj

**Key words:** Plasma simulation, MHD, particle-in-cell, implicit methods.

---

## 1 Introduction

Plasma dynamics span a large range of time and space scales, and no one model can cover them all. For very fast time scales and very small spatial scales, classical plasma simulations work very well, but at the cost of resolving all scales and consuming vast amounts of computing power. Magnetofluid (MHD) calculations model large scales and long times, but eliminate kinetic effects. In the landscape between, there are reduced models, such as hybrid and gyrokinetic models, and there are implicit methods, which

---

\*Corresponding author. *Email addresses:* jerrybrackbill@comcast.net (J. U. Brackbill), Giovanni.Lapenta@wis.kuleuven.be (G. Lapenta)

extend plasma simulations to larger scales while retaining the contributions of kinetic electrons. An increase in applicability of any of these methods would be useful.

Here we ask if implicit methods can be extended to problems on MHD time scales. Do the equations become so inaccurate and difficult to solve that there is no value in doing so? Specifically, we ask if the field equations become substantially more difficult to solve, and whether stochastic heating can be controlled as one increases time and length scales. There is a recent review of implicit simulation [23], to which we direct readers wishing a more comprehensive review. On the other hand, we include some details that have not previously been reported in order to proceed with our analysis.

Implicit simulation methods were invented by Mason [25] and Denavit [13], who combined fluid and kinetic models of electrostatic plasmas to bypass stability constraints imposed by explicit-in-time methods. Explicit stability constraints require that

$$\omega_{pe}\Delta t < 2, \quad h/(u_e/\omega_{pe}) < 1,$$

and that  $c\Delta t/h < 1$  for electromagnetic plasma interactions, where  $\omega_{pe}$  is the electron plasma frequency,  $c$  is the speed of light,  $\Delta t$  is the time step, and  $h$  is the minimum resolved length scale. The minimum resolved scale,  $h$ , must be less than the electron Debye length,  $u_e/\omega_{pe}$ , to avoid the finite grid instability [18, 24]. Mason and Denavit noted the solution of the field equations requires only the first few moments of the particle distribution, and that the evolution of the moments can be predicted using a much smaller system of equations than is required to advance the particle orbits. By solving implicit-in-time moment and field equations self-consistently, the implicit moment method advances the particle solutions just once each cycle, as in an explicit solution, while retaining the superior numerical stability properties of a fully implicit method.

The moment equations are derived from an expansion of the moments about their initial values in powers of  $u_e\Delta t/h$ , where  $u_e$  is the root mean square electron speed. The accuracy of the expansion requires that  $u_e\Delta t/h < 1$ , but

$$u_e\Delta t/h = (u_e/\omega_{pe})/h \times \omega_{pe}\Delta t.$$

Thus  $\Delta t$  can be increased if  $h$  is also increased.  $h$  can be increased because implicit methods are less prone to the finite-grid-instability than explicit methods [3], and  $\Delta t$  can be increased because of the unconditional stability of implicit methods. The advantage of the implicit solution is most evident in the scaling of the cost of a simulation with the ion/electron mass ratio. Given a problem on ion time and space scales with

$$T = n\omega_{pi}^{-1}, \quad L = l(c/\omega_{pi}),$$

the explicit/implicit cost ratio scales as  $(m_i/m_e)^{3/2}$ . Data on the relative cost of explicit and implicit calculations in 2 dimensions is given in Table 1 of [31]. It should be noted that the explicit calculations resolve all scales, and the implicit calculations do not. There is much more detail in the explicit results. On the other hand, explicit calculations cost

up to 40000 times as much for the same problem. That means that explicit calculations with physical ion/electron mass ratios are still too costly to undertake, and computations in 3-dimensions are even more impossible.

Low-frequency, electromagnetic simulation has had wide application. With the implicit moment code, VENUS, simulations of the interaction of a  $CO_2$  laser with a target revealed the lateral transport of electrons caused by the propagation of self-generated magnetic fields across the target surface [10, 36]. Simulations of quasi-parallel [28] and quasi-perpendicular [11] collisionless shocks in two dimensions revealed the unsteady nature of the shocks and mechanisms for heating that had not previously been observed. Simulations of the lower hybrid drift instability in a Harris sheet identified electron heating as the primary saturation mechanism, one which causes saturation at much lower amplitudes than previously estimated [4]. More recent simulations are referenced in [23].

In all of these calculations, the motion is non-relativistic,  $u_e/c \approx \epsilon$ , where  $\epsilon < 1$ , and electromagnetic waves are not resolved,  $c\Delta t/h > 1$ . The electron Debye length is small compared with minimum resolved spatial scales,  $(u_e/\omega_{pe})/h \approx \epsilon$ , but the collisionless skin depth is not necessarily small,  $(c/\omega_{pe})/h \approx 1$ . However, the accuracy condition,  $|\mathbf{u}|\Delta t/h \approx 1$ , allows a large time step,

$$(\omega_{pe}\Delta t) \approx 1/\epsilon^2.$$

Here, we review the current implicit moment algorithm, as it is implemented in CELESTE, analyze its properties, with particular attention to nonlinear stability, solution of the field equations in the MHD limit, and energy conservation. We conclude with some results for a collisional plasma, showing that collisions reduce stochastic heating when the collision frequency is high.

## 2 Implicit plasma simulation

### 2.1 Implicit-in-time equations

Implicit plasma simulation means the solution of a system of implicit-in-time equations with time steps,  $\Delta t$ , that are typically much larger than those allowed by explicit simulations. Implicit equations may take many forms, but for reasons that will become more evident when we examine certain features of the solutions, we will discuss a first order formulation. Where  $\mathbf{E}$  and  $\mathbf{B}$  are the electric and magnetic fields, and  $\rho$  and  $\mathbf{J}$  are the charge and current density, and with the convention, that  $\mathbf{E}^n \equiv \mathbf{E}(n\Delta t)$ , we write semi-discrete approximations to Faraday's law

$$\nabla \times \mathbf{E}^{n+\theta} + \frac{\mathbf{B}^{n+1} - \mathbf{B}^n}{c\Delta t} = 0, \quad (2.1)$$

and Ampere's law

$$\nabla \times \mathbf{B}^{n+1/2} - \frac{\mathbf{E}^{n+1} - \mathbf{E}^n}{c\Delta t} = \frac{4\pi}{c} \mathbf{J}^{n+1/2}. \quad (2.2)$$

The fractional time levels are computed by linear interpolation. For example,

$$\mathbf{E}^{n+\theta} = \theta \mathbf{E}^{n+1} + (1-\theta) \mathbf{E}^n.$$

The choice of time levels is an attempt to satisfy a number of constraints. For example, in Eq. (2.2),  $\mathbf{B}$  on the LHS and  $\mathbf{J}$  on the RHS are at the same time level because, in the low-frequency, quasineutral limit,  $\mathbf{E}$  is slowly varying and

$$4\pi\mathbf{J} \approx c\nabla \times \mathbf{B}.$$

Thus it would be inconsistent to have  $\mathbf{J}$  and  $\mathbf{B}$  at different times. If  $\mathbf{J}$  is evaluated at any time other than  $n+1/2$ , strong damping of gyromotion results. Thus, both  $\mathbf{J}$  and  $\mathbf{B}$  must be at  $n+1/2$ . Tanaka argues that this choice, with  $\mathbf{B}$  in Eq. (2.2) and  $\mathbf{E}$  in Eq. (2.1) at different times incorrectly computes the ponderomotive force [35, p. 120]. However, his argument applies to high-frequency, electromagnetic waves where  $\mathbf{J}$  and  $\mathbf{E}$  dependent terms nearly balance in Eq. (2.2).

The magnetic field is solenoidal,

$$\nabla \cdot \mathbf{B}^n = 0, \quad (2.3)$$

and charge is conserved,

$$\nabla \cdot \mathbf{E}^n = 4\pi\rho^n. \quad (2.4)$$

The particle velocity,  $\mathbf{u}_p$ , can be written,

$$\mathbf{u}_p^{n+1} = \mathbf{u}_p^n + \left( \left( \frac{q}{m} \right)_s \mathbf{E}^{n+\theta}(\mathbf{x}_p^{n+1/2}) + \mathbf{u}_p^{n+1/2} \times \boldsymbol{\Omega}_{ps} \right) \Delta t - \mathcal{C}_{ps} \Delta t, \quad (2.5)$$

where the cyclotron frequency is defined by,

$$\boldsymbol{\Omega}_{ps} \equiv \left( \frac{q}{m} \right)_s \frac{\mathbf{B}^n(\mathbf{x}_p^{n+1/2})}{c}, \quad (2.6)$$

and the simple collision model,

$$\mathcal{C}_{ps} = -\nu_s \left( \mathbf{u}_p^{n+1/2} - \mathbf{U}_s^{n+1/2}(\mathbf{x}_p^{n+1/2}) \right), \quad (2.7)$$

is employed. The center-of-mass velocity,  $\mathbf{U}_s$  is defined below.

The time at which  $\boldsymbol{\Omega}_{ps}$  is evaluated anticipates the form in which we write Ohm's law, Eq. (3.8), below. The particle position is given by,

$$\frac{\mathbf{x}_p^{n+1} - \mathbf{x}_p^n}{\Delta t} = \mathbf{u}_p^{n+1/2}. \quad (2.8)$$

All of the particles of species  $s$  will have the same charge/mass ratio,  $(q/m)_s$  and collision frequency,  $\nu_s$ . However, each particle may have a different charge,  $q_p$ , and mass  $m_p$ .

The particles also have a finite size, with the distribution of their properties in space defined by a shape function,  $S(\mathbf{x})$ , which is a positive, symmetric function with normalization,

$$\int_{\mathcal{D}} S(\mathbf{x}) dV = 1. \quad (2.9)$$

The shape function has bounded support, such that  $S(\mathbf{x}) = 0$  for  $|\mathbf{x}| > h$ .

The shape function allows us to compute particle moments by summing the contributions of charge and current at each point in space. For example, the charge density,  $Q^n$ , and current density,  $\mathbf{J}^{n+1/2}$ , are

$$\begin{aligned} Q^n(\mathbf{x}) &= \sum_p q_p S(\mathbf{x} - \mathbf{x}_p^n), \\ \mathbf{J}^{n+1/2}(\mathbf{x}) &= \sum_p q_p \mathbf{u}_p^{n+1/2} S(\mathbf{x} - \mathbf{x}_p^{n+1/2}). \end{aligned} \quad (2.10)$$

The time at which each of the moments is evaluated anticipates its use below.

The center of mass velocity is defined such that,

$$\sum_p q_p (\mathbf{u}_p - \mathbf{U}_s(\mathbf{x})) S(\mathbf{x} - \mathbf{x}_p) = 0. \quad (2.11)$$

One last detail. Because the particles have finite size, we must specify what we mean by  $\mathbf{E}(\mathbf{x}_p)$ . Energy conservation constrains the definition in the following way.

The energy of the system is the sum of field and particle energies,

$$\mathcal{E} = \int_{\mathcal{D}} \frac{1}{8\pi} (\mathbf{E}^2 + \mathbf{B}^2) dV + \sum_p \frac{1}{2} m_p \mathbf{u}_p^2. \quad (2.12)$$

The change in energy over a time step is computed by forming the inner product of  $\mathbf{E}^{n+\theta}$  with Faraday's law, Eq. (2.1),  $\mathbf{B}^{n+1/2}$  with Ampere's law, Eq. (2.2), and  $m_p \mathbf{u}_p^{n+1/2}$  with the particle acceleration, Eq. (2.5) and summing the results. The change in the field energy is,

$$\begin{aligned} \mathcal{E}_F^{n+1} - \mathcal{E}_F^n &= -\Delta t \int_{\mathcal{D}} \left[ \frac{c}{4\pi} \nabla \cdot (\mathbf{E}^{n+\theta} \times \mathbf{B}^{n+1/2}) + \mathbf{J}^{n+1/2} \cdot \mathbf{E}^{n+\theta} \right. \\ &\quad \left. + \frac{\theta-1/2}{4\pi} (\mathbf{E}^{n+1} - \mathbf{E}^n)^2 \right] dV. \end{aligned} \quad (2.13)$$

The last term in the integrand is the error due to de-centering the equations, which is dissipative when  $\theta > 1/2$ .

The work done by the fields on the particles follows from the definition of the current density,

$$\int_{\mathcal{D}} \mathbf{J}^{n+1/2} \cdot \mathbf{E}^{n+\theta} dV = \sum_p q_p \mathbf{u}_p^{n+1/2} \cdot \int_{\mathcal{D}} \mathbf{E}^{n+\theta} S(\mathbf{x} - \mathbf{x}_p^{n+1/2}) dV. \quad (2.14)$$

The change in the particle energy due to the action of the fields is,

$$\mathcal{E}_{KE}^{n+1} - \mathcal{E}_{KE}^n = \sum_p q_p \mathbf{u}_p^{n+1/2} \cdot q_p \mathbf{E}^{n+\theta}(\mathbf{x}_p^{n+1/2}). \quad (2.15)$$

The change in particle kinetic energy due to collisions is,

$$\mathcal{E}_{collisions}^{n+1} - \mathcal{E}_{collisions}^n = -\nu_s \sum_p m_p (\mathbf{u}_p - \mathbf{U}_s)^2 \Delta t. \quad (2.16)$$

To conserve energy, the particle kinetic energy dissipated by collisions is added to a particle internal energy,  $m_p e_p$ . The work done by the fields and the change in particle energy due to the action of the fields must be equal, and they are if we define the field at the particle by the convolution,

$$\mathbf{E}^{n+\theta}(\mathbf{x}_p^{n+1/2}) \equiv \int_D \mathbf{E}^{n+\theta}(\mathbf{x}) \mathcal{S}(\mathbf{x} - \mathbf{x}_p^{n+1/2}) dV. \quad (2.17)$$

The magnetic field at the particle is defined similarly.

### 3 The implicit-moment approximation

#### 3.1 Ohm's law

We now identify the linear dependence of  $\mathbf{J}^{n+1/2}$  upon  $\mathbf{E}^{n+\theta}$ , and move it to the LHS of Eq. (2.2). This results in a linear equation with only known quantities on the RHS. To do so, we expand  $\mathbf{J}^{n+1/2}$  in powers of  $\epsilon = |\mathbf{u}| \Delta t / h$ , and discard terms of  $\mathcal{O}(\epsilon^2)$  and higher.

The particle velocity equation, Eq. (2.5), with collisions, is simplified,

$$\mathbf{u}_p^{n+1/2} = \tilde{\mathbf{u}}_p + \left( \left( \frac{q}{m} \right)_s \mathbf{E}^{n+\theta}(\mathbf{x}_p^{n+1/2}) + \mathbf{u}_p^{n+1/2} \times \boldsymbol{\Omega}_{ps} \right) \frac{\tau_s}{2}, \quad (3.1)$$

by defining an effective collision time,

$$\tau_s \equiv \frac{\Delta t}{1 + \nu_s \Delta t / 2}, \quad (3.2)$$

and explicit displacement rate,

$$\tilde{\mathbf{u}}_p \equiv \mathbf{u}_p^n - \left( \mathbf{u}_p^n - \mathbf{U}_s^{1/2} \right) \nu_s \frac{\tau_s}{2}. \quad (3.3)$$

We note that

$$\lim_{\nu_s \Delta t \rightarrow 0} \tilde{\mathbf{u}}_p = \mathbf{u}_p^n, \quad \lim_{\nu_s \Delta t \rightarrow \infty} \mathbf{u}_p^{n+1/2} = \mathbf{U}_s^{1/2},$$

and that  $\tau \leq \Delta t$  for all values of  $\nu_s$  and  $\Delta t$ .

The electric field at the particle position, Eq. (2.17), and the current density, Eq. (2.10),  $\mathcal{S}$  are defined with  $\mathbf{x}_p^{n+1/2}$ . This dependence can be expanded in powers of  $\epsilon$  about  $\mathbf{x}_p^n$ . Because  $\mathcal{S}$  is symmetric, its derivative is anti-symmetric, and

$$\mathcal{S}(\mathbf{x}-\mathbf{x}_p^{n+1/2}) = \left( \mathcal{S}(\mathbf{x}-\mathbf{x}_p^n) - \frac{\Delta t}{2} \mathbf{u}_p^{n+1/2} \cdot \nabla_{\mathbf{x}} \mathcal{S}(\mathbf{x}-\mathbf{x}_p^n) \right) + \mathcal{O}(\epsilon^2). \quad (3.4)$$

The electric and magnetic fields in Eq. (3.1) are evaluated at a time-advanced position of the particle,  $\mathbf{x}_p^{n+1/2}$ . But if we substitute Eq. (3.4) into the definition of  $\mathbf{E}(\mathbf{x}_p)$ , for example,

$$\mathbf{E}^{n+\theta}(\mathbf{x}_p^{n+1/2}) = \int_D \mathbf{E}^{n+\theta}(\mathbf{x}) \mathcal{S}(\mathbf{x}-\mathbf{x}_p^n) dV + \mathcal{O}(\epsilon), \quad (3.5)$$

we see that the substitution of fields evaluated at  $\mathbf{x}_p^n$  into Eq. (3.1) introduces an error of  $\mathcal{O}(\epsilon)^2$  into its solution. A first-order approximation to Eq. (2.5) is thus given by evaluating the fields at the  $n$  time level particle positions,

With this approximation, Eq. (2.5) can be solved for  $\mathbf{u}_p^{n+1/2}$  by resolving it into components parallel and perpendicular to  $\mathbf{B}$ , which yields

$$\mathbf{u}_p^{n+1/2} = \mathbf{\Pi}_{ps} \cdot \left( \tilde{\mathbf{u}}_p + \left( \frac{q}{m} \right)_s \mathbf{E}^{n+\theta}(\mathbf{x}_p^n) \frac{\tau_s}{2} \right), \quad (3.6)$$

where the tensor  $\mathbf{\Pi}$  is given by

$$\mathbf{\Pi}_{ps} = \frac{\left[ \mathbf{I} - \mathbf{I} \times \mathbf{\Omega}_{ps} \frac{\tau_s}{2} + \mathbf{\Omega}_{ps} \mathbf{\Omega}_{ps} \left( \frac{\tau_s}{2} \right)^2 \right]}{1 + \left( \mathbf{\Omega}_{ps} \frac{\tau_s}{2} \right)^2}. \quad (3.7)$$

with  $\mathbf{\Pi}_{ps}$  evaluated with  $\mathbf{B}^n(\mathbf{x}_p^n)$

We sum over the set of particles of species

$$P_s = \{ P_s : p \in N, (q_p / m_p) = (q / m)_s \}$$

and substitute from definition of moments to derive Ohm's law

$$\mathbf{J}_s^{n+1/2}(\mathbf{x}) \approx \hat{\mathbf{J}}_s + \hat{\sigma} \cdot \mathbf{E}^{n+\theta}. \quad (3.8)$$

We approximate the current,  $\hat{\mathbf{J}}$ , by

$$\hat{\mathbf{J}}_s \equiv \sum_{p \in P_s} q_p \mathbf{\Pi}_p^n \cdot \tilde{\mathbf{u}}_p \mathcal{S}(\mathbf{x}-\mathbf{x}_p^n) - \sum_{p \in P_s} q_p \mathbf{\Pi}_p^n \cdot \tilde{\mathbf{u}}_p \mathbf{\Pi}_p^n \cdot \tilde{\mathbf{u}}_p \cdot \nabla_{\mathbf{x}} \mathcal{S}(\mathbf{x}-\mathbf{x}_p^n) \frac{\Delta t}{2}, \quad (3.9)$$

and the conductivity,  $\hat{\sigma}$ , by

$$\hat{\sigma}_s \cdot \mathbf{E}^{n+\theta} \equiv \left( \frac{q}{m} \right)_s \sum_{p \in P_s} q_p \mathbf{\Pi}_p \cdot \left( \int_D \mathbf{E}^{n+\theta}(\mathbf{x}') \mathcal{S}(\mathbf{x}'-\mathbf{x}_p^n) dV' \right) \mathcal{S}(\mathbf{x}-\mathbf{x}_p^n) \frac{\Delta t}{2}. \quad (3.10)$$

Because of Eq. (2.11),  $\Delta t$  replaces  $\tau_s$  in the definition of  $\Pi_{ps}$ . In other words, collisions have no effect on the mean flow for each species. We note that if we were to evaluate  $\Pi_p$  with  $\mathbf{B}^{n+1/2}$  in Eq. (3.7), it would require our showing that  $\mathbf{B}^{n+1/2} - \mathbf{B}^n$  is small in some sense. Only then could we still write Ohm's law with a linear dependence on  $n+1/2$  time level variables as given by Eq. (3.8). If  $\mathbf{B}^{n+1/2} - \mathbf{B}^n$  were large, there would be the possibility of seriously degrading the accuracy of the field solution.

Consistent with Eq. (2.11), the center of mass velocity appearing in the collision term, Eq. (8) is evaluated for each species using Eq. (3.8),

$$\mathbf{U}_s^{n+1/2} = \frac{\mathbf{J}_s^{n+1/2}}{Q_s^n}. \quad (3.11)$$

The total current, for example, is computed by summing the species currents,

$$\mathbf{J}^{n+1/2} = \sum_s \mathbf{J}_s^{n+1/2}. \quad (3.12)$$

Unless there are collisions between species, there is no resistance to current flow, and the conductivity is more accurately called a susceptibility, at which point Eq. (3.8) invites a comparison with the direct implicit formulation [19, 20]. Mason comments there is an equivalence between direct and moment methods under certain circumstances [26, pp248-249].

### 3.2 Assignment functions

We now consider a set of points  $\mathbf{x}_v = \{\mathbf{x}_v : \mathbf{x}_v \in D, v = 1, \dots, N_v\}$ , with which we associate a vertex volume  $V_v$  such that

$$\sum_v V_v = \int_D dV.$$

We define an assignment function by integrating the particle shape function over this volume,

$$\mathcal{A}(\mathbf{x}_v - \mathbf{x}) \equiv \int_{V_v} \mathcal{S}(\mathbf{x}' - \mathbf{x}) dV'. \quad (3.13)$$

The assignment function is a partition of unity, and

$$1 = \sum_v \mathcal{A}(\mathbf{x}_v - \mathbf{x}).$$

It is trivial to show that the integral of  $\mathcal{A}$  over  $D$  is,

$$\int_D \mathcal{A}(\mathbf{x} - \mathbf{x}_v) dV = V. \quad (3.14)$$

Vertex values of the moments are defined to be the average of the moments given by Eq. (2.10) over  $V_v$ . The current density is,

$$\hat{\mathbf{J}}_{vs} \equiv \frac{1}{V_v} \left[ \sum_{p \in P_s} q_p \Pi_p^n \cdot \tilde{\mathbf{u}}_p \mathcal{A}(\mathbf{x}_v - \mathbf{x}_p^n) - \sum_{p \in P_s} q_p \Pi_p^n \cdot \tilde{\mathbf{u}}_p \Pi_p^n \cdot \tilde{\mathbf{u}}_p \cdot \nabla_{\mathbf{x}_v} \mathcal{A}(\mathbf{x}_v - \mathbf{x}_p^n) \frac{\Delta t}{2} \right]. \quad (3.15)$$

We introduce a functional representation for the field,

$$\sum_v \mathbf{E}_v \mathcal{A}(\mathbf{x}_v - \mathbf{x}) = \int_D \mathbf{E}(\mathbf{x}') \mathcal{S}(\mathbf{x}' - \mathbf{x}) dV', \quad (3.16)$$

which, using Eq. (3.14), satisfies the conservation law,

$$\sum_v \mathbf{E}_v V_v = \int_D \mathbf{E}(\mathbf{x}) dV. \quad (3.17)$$

Substituting Eq. (3.16) into Eq. (3.10), and integrating over  $V_v$ , gives us a conductivity matrix,

$$\sum_{v'} \hat{\sigma}_{vv's} \cdot \mathbf{E}_{v'}^{n+\theta} \equiv \frac{1}{V_v} \left( \frac{q}{m} \right)_s \sum_{p \in P_s} q_p \Pi_p \cdot \sum_{v'} \mathbf{E}_{v'}^{n+\theta} \mathcal{A}(\mathbf{x}_{v'} - \mathbf{x}_p^n) \mathcal{A}(\mathbf{x}_v - \mathbf{x}_p^n) \frac{\Delta t}{2}. \quad (3.18)$$

### 3.3 Solution on a grid

We will now describe a ‘staggered mesh method’, which has several very nice properties, among them that they produce finite difference approximations that satisfy conservation laws and preserve vector identities. The approximations were first developed by Schultz [32], and extended to three dimensions by Brackbill [2].

We use the functional representation for  $\mathbf{E}$  given by Eq. (3.16). to derive a difference approximation to Faraday’s law by integrating over a control volume  $V_c$ ,

$$\sum_v \int_{V_c} \nabla \mathcal{A}(\mathbf{x} - \mathbf{x}_v) dV \times \mathbf{E}_v^{n+\theta} + \frac{\int_{V_c} (\mathbf{B}^{n+1} - \mathbf{B}^n) dV}{c\Delta t} = 0. \quad (3.19)$$

We introduce  $V_c$  as a real geometric object, and

$$\sum_c V_c = V_D.$$

In fact, we can restate the definition of  $V_v$  given by Eq. (3.14),

$$V_v = \sum_c \int_{V_c} \mathcal{A}(\mathbf{x} - \mathbf{x}_v) dV. \quad (3.20)$$

With  $\mathbf{B}_c V_c \equiv \int_{V_c} \mathbf{B} dV$ , our approximation to Faraday’s law is,

$$\frac{1}{V_c} \sum_v \mathbf{g}_{cv} \times \mathbf{E}_v^{n+\theta} + \frac{\mathbf{B}_c^{n+1} - \mathbf{B}_c^n}{c\Delta t} = 0, \quad (3.21)$$

where

$$\mathbf{g}_{cv} \equiv \int_{V_c} \nabla \mathcal{A}(\mathbf{x} - \mathbf{x}_v) dV. \quad (3.22)$$

The value of the integral is determined analytically. Any error in the difference equation comes from the approximation error in the functional representation for  $\mathbf{E}$ , given by Eq. (3.16).

We derive an approximation to Ampere's law by the method of virtual work. First, we define the electromagnetic field energy by,

$$\mathcal{E} = \frac{1}{8\pi} \left[ \sum_c \mathbf{B}_c \cdot \mathbf{B}_c V_c + \sum_v \mathbf{E}_v \cdot \mathbf{E}_v V_v \right]. \quad (3.23)$$

The change in  $\mathcal{E}$  over a time step is computed by forming the inner product of  $\mathbf{B}$  with Faraday's law, Eq. (3.21), and of  $\mathbf{E}$  with Ampere's law, Eq. (2.2). The magnetic energy from Eq. (3.21) is,

$$\Delta \mathcal{E}_B = - \sum_c \mathbf{B}_c^{n+1/2} \cdot \sum_v \mathbf{g}_{cv} \times \mathbf{E}_v^{n+\theta}. \quad (3.24)$$

The change in the electric field energy,  $\mathcal{E}_E$  is computed from Ampere's law, Eq. (2.2), similarly to the magnetic field energy. We replace  $\mathbf{E} \cdot \nabla \times \mathbf{B}$  by the RHS of Eq. (3.27), with opposite sign to force cancellation,

$$\Delta \mathcal{E}_E = c \Delta t \sum_c \mathbf{B}_c^{n+1/2} \cdot \sum_v \mathbf{g}_{cv} \times \mathbf{E}_v^{n+\theta} - \sum_v \left[ \Delta t \mathbf{E}_v^{n+\theta} \cdot \mathbf{J}_v^{n+1/2} - \frac{(\theta-1/2)}{4\pi} (\mathbf{E}^{n+1} - \mathbf{E}^n)^2 \right] V_v, \quad (3.25)$$

and the total energy change is equal to the work done on the plasma less the dissipation that results when  $\theta > 1/2$ ,

$$\mathcal{E} = - \sum_v \left[ \Delta t \mathbf{E}_v^{n+\theta} \cdot \mathbf{J}_v^{n+1/2} - \frac{(\theta-1/2)}{4\pi} (\mathbf{E}^{n+1} - \mathbf{E}^n)^2 \right] V_v. \quad (3.26)$$

Using a vector identity and inverting the order of summation, we can rewrite the first term on the RHS of Eq. (3.25),

$$\sum_c \mathbf{B}_c^{n+1/2} \cdot \sum_v \mathbf{g}_{cv} \times \mathbf{E}_v^{n+\theta} = - \sum_v \mathbf{E}_v^{n+\theta} \cdot \sum_c \mathbf{g}_{cv} \times \mathbf{B}_c^{n+1/2}. \quad (3.27)$$

We note that unless we explicitly set boundary conditions, the Poynting flux at the boundary vanishes. We can now factor  $\mathbf{E}_v^{n+\theta} V_v$  from Eq. (3.25), and since we can replace  $\mathbf{E}_v$  by an arbitrary vector, the difference equation that must be solved for each value of  $v$  is,

$$\mathbf{E}_v^{n+1} - \mathbf{E}_v^n = \frac{1}{V_v} c \Delta t \sum_c - \mathbf{g}_{cv} \times \mathbf{B}_c^{n+1/2} - 4\pi \Delta t \mathbf{J}_v^{n+1/2}. \quad (3.28)$$

The magnetic field can be eliminated between Faraday's and Ampere's laws to give an equation for the electric field. We replace  $\mathbf{J}^{n+1/2}$  with the linearized Ohm's law, Eq. (3.8), using the conductivity, Eq. (3.18), in its lumped form, Eq. (4.5). The result is,

$$\begin{aligned} & \frac{\theta}{2} (c \Delta t)^2 \frac{1}{V_v} \sum_c - \mathbf{g}_{cv} \times \frac{1}{V_c} \sum_{c'} \mathbf{g}_{c'v} \times \mathbf{E}_{c'}^{n+\theta} + (\mathbf{I} + 4\pi \theta \Delta t \sigma_v) \cdot \mathbf{E}_v^{n+\theta} \\ & = \mathbf{E}_v^n + (c \theta \Delta t) \left( \frac{1}{V_v} \sum_c - \mathbf{g}_{cv} \times \mathbf{B}_c^n - \frac{4\pi}{c} \hat{\mathbf{J}}_v \right). \end{aligned} \quad (3.29)$$

## 4 Analysis

Perhaps this section might better be titled 'living with CELESTE', for we discuss how to manage plasma heating and how to solve the field equations. On the other hand, the problems we consider are generic problems in plasma simulation, for example, plasma heating and the solution of the field equations. We also discuss collisions as a means to do fluid modeling with an implicit plasma simulation method.

### 4.1 Plasma heating

Cohen *et al.* made a systematic study of numerical heating for the direct implicit method [9], in which they map the energy error as a surface in  $\Delta t$ - $h$  parameter space. They show that energy increases because of plasma heating except in a narrow band

$$0.5 < u_e \Delta t / h < 1.0,$$

even when the numerical scheme is dissipative.

The underlying cause of heating is the fluctuations in charge that result from using small numbers of simulation particles to model the plasma. Hockney [14] gives a particle heating rate for a stochastic process,

$$\frac{d\mathcal{E}_K}{dt} = \frac{q^2}{m} \langle E^2 \rangle \tau_{correlation}, \quad (4.1)$$

and an estimate of the stochastic field from kinetic theory,

$$\frac{\langle E^2 \rangle}{\mathcal{E}_K} \approx \frac{1}{2} \frac{0.1}{n \lambda_{De}^2}. \quad (4.2)$$

These results suggest that implicit simulations with  $\omega_{pe} \Delta t \approx 1$  and  $h / \lambda_{De} < 1$  should suffer rapid heating.

The stochastic field enters the computation cycle through a correction of the electric field at the beginning of each cycle to make it consistent with the charge density computed from Eq. (2.10). A correction potential is computed from,

$$\nabla \cdot \nabla \phi = \nabla \cdot [\mathbf{E}^n - 4\pi Q^n]. \quad (4.3)$$

The stochastic field energy is measured by the correction potential,

$$\int_D \delta E^2 dV = \int_D \nabla \phi^2 dV.$$

In Fig. 1, we show a history of the total, particle, and magnetic field energies for a Harris current sheet equilibrium [22,31] in the plane perpendicular to the magnetic field. The x-directed magnetic field reverses polarity at the center of the current sheet where

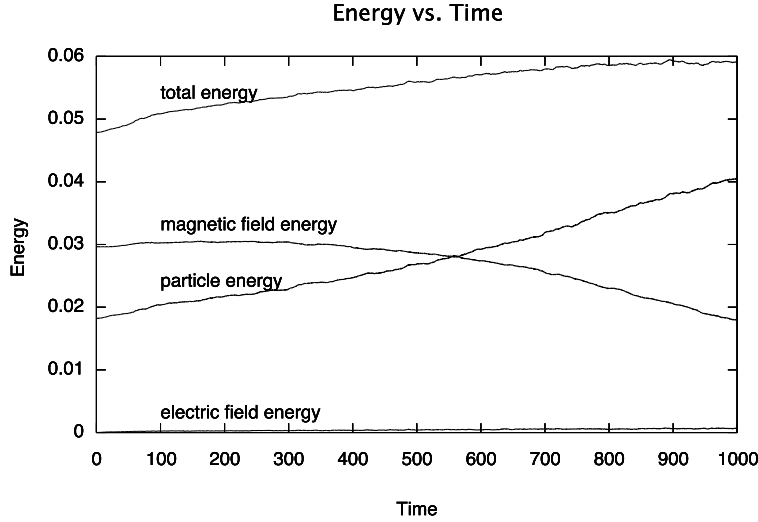


Figure 1: The total (top curve) and particle (third from top) energies increase, while the magnetic field energy (second from top) decreases. Time in this and all succeeding plots is in units of  $\omega_{pi}^{-1}$ . The calculation with  $\omega_{pi}\Delta t=0.1$ ,  $m_i/m_e=180$ ,  $\theta=0.5$  and 25 electrons per cell uses the GEM challenge equilibrium, but is in a plane perpendicular to the magnetic field. The decrease in magnetic field energy and some of the increase in particle energy is a result of the action of a lower hybrid drift instability. The remainder of the particle heating, which occurs at a roughly constant rate, is consistent with a stochastic cause.

the plasma density has its maximum value. The computation is performed on a grid with 32 zones in  $y$  and 16 zones in  $z$ , and mesh spacing  $h_x=0.4c/\omega_{pi}$  and  $h_z=0.5c/\omega_{pi}$ , where  $y$  is a periodic coordinate and  $z$  is the direction of variation for the equilibrium. The time step is  $\omega_{pi}\Delta t=0.1$ , and  $\theta=0.5$ , so the equations are second-order in the time step, and non-dissipative. The ion/electron mass ratio is 180. The mean electron particle displacement each time step is  $u_e\Delta t/h=0.025$ .

In this problem, a lower hybrid drift instability causes electron heating at the expense of magnetic field energy. With the implicit calculation, the total energy increases; numerical particle heating accounts for the increase. With the numerical parameters above, the 'stochastic' field, Fig. 2, is smaller than Hockney's estimate, Eq. (4.2). The ratio

$$\langle E^2 \rangle / \mathcal{E}_K \approx 0.015.$$

(Our measure is the integral of  $\nabla\phi \cdot \nabla\phi$  over the domain. The increase over time in the measure is caused by particle heating.) This gives

$$n\lambda_{De}^2 \approx 10.$$

The estimated  $n\lambda_{De}^2$  from the relation,

$$\frac{u_e\Delta t}{h} = \left(\frac{m_i}{m_e}\right)^{1/2} \frac{\lambda_{De}}{h} \omega_{pi}\Delta t, \quad (4.4)$$

$\lambda_{De}/h \approx 0.02$ . With 25 electrons per cell, there are only 1/100 particle per Debye circle! Evidently, the implicit algorithm reduces the stochastic field to a value that would require a much larger number of particles to achieve with an explicit code.

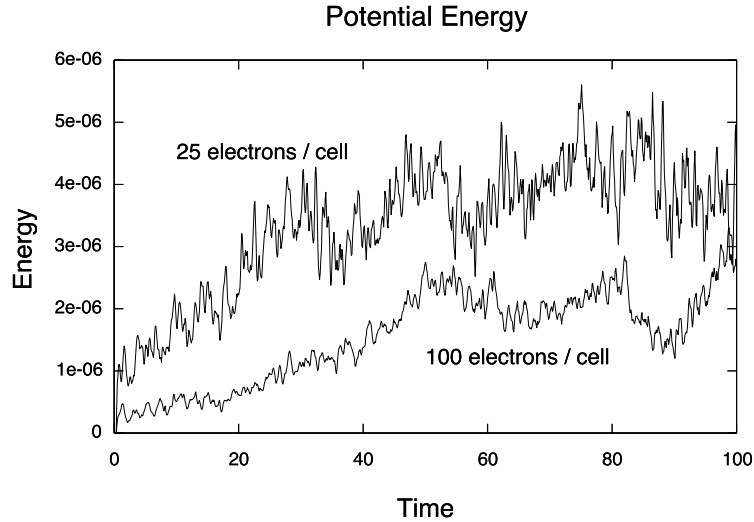


Figure 2: The energy in the correction field gives a measure of the 'stochastic' field, since the only source should be fluctuations in charge density. The 'stochastic' field scales as the  $n_e^{1/2}$ , where  $n_e$  is the number of electrons per cell. With 100 electrons per cell, the correction field is half the value with 25 electrons per cell.

If we increase the number of particles to 100 electrons per cell, the stochastic field is roughly halved, Fig. 2, as does  $n^{-1/2}$ . If the implicit equations are solved as backward-Euler equations,  $\theta = 1$ , there is numerical dissipation of the electric field, Fig. 3, which improves overall energy conservation by partially balancing the stochastic field contribution. The numerical dissipation is largest for high frequency, short wavelength modes, and selectively filters the stochastic fields.

### 4.2 Other energy terms

The work done by the field on the particles, Eq. (2.14), and the work done on the particles by the fields, Eq. (2.15) balance to  $\mathcal{O}(u_e \Delta t / h)^2$ , with the estimated conductivity in Ohm's law, Eq. (3.18). However, the conductivity matrix occupies an enormous amount of computer memory. For standard area-weighting assignment functions, the storage of the conductivity matrix in 3 dimensions requires  $9 \times 27$  arrays (times the number of species). Storage is reduced to 9 arrays if one uses a 'lumped conductivity',

$$\sigma_v = \sum_{v'} \sigma_{vv'}, \tag{4.5}$$

but this introduces an error.

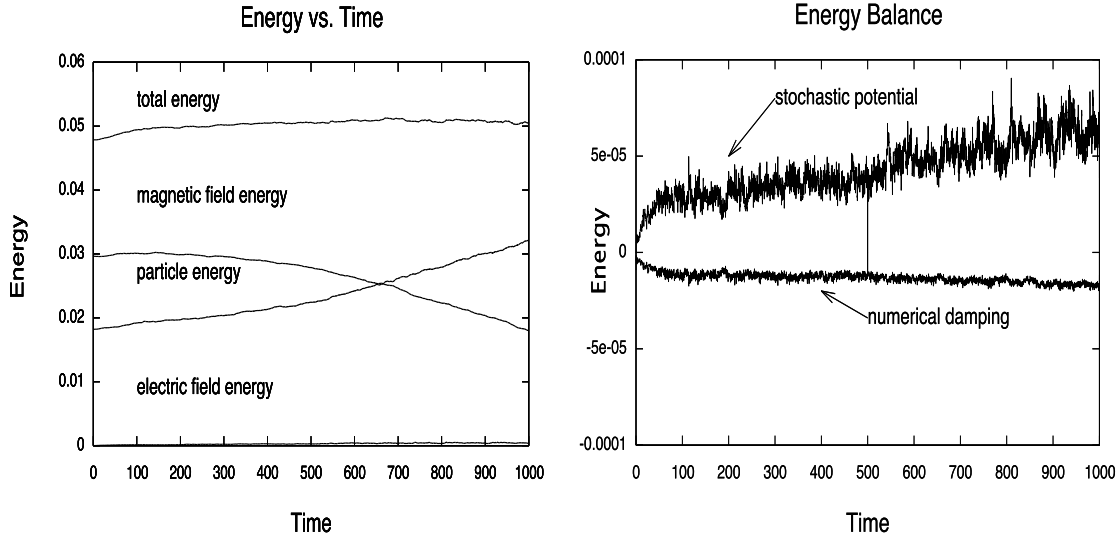


Figure 3: When the calculation shown in Fig. 1 is repeated with  $\theta=1.$ , numerical damping, defined in Eq. (2.13), is sufficient to greatly improve overall energy conservation (left), but is small when compared directly with the stochastic heating rate (right).

Recall that the conductivity matrix in Eq. (3.18) is derived directly from the particle equations of motion, to which it is an approximation of  $\mathcal{O}(u_e \Delta t / h)^2$ . To this order, there is no error in the contributions of  $\hat{\mathbf{j}}$ , Eq. (3.15). Thus, the error caused by lumping is,

$$\delta \mathcal{E}_{\mathbf{J} \cdot \mathbf{E}} = -\frac{1}{V_v} \left( \frac{q}{m} \right)_s \sum_{v'} \mathbf{E}_{v'}^{n+\theta} \cdot \sum_{p \in P_s} q_p \mathbf{\Pi}_p (\sigma_v \delta_{v,v'} - \sigma_{vv'}) + \mathcal{O}(u_e \Delta t / h)^2. \quad (4.6)$$

Also recall that

$$\mathbf{E}(\mathbf{x}_p) = \sum_v \mathbf{E}_v \mathcal{A}(\mathbf{x}_v - \mathbf{x}_p).$$

Second, we note that  $\mathbf{E}(\mathbf{x}_p) \cdot \mathbf{\Pi}_p \cdot \mathbf{E}(\mathbf{x}_p) \geq 0$  because the antisymmetric components give no contribution. Since  $\mathcal{A} \geq 0$ , the coefficient of each term in the sum over  $p$  is positive. We now must determine the sign of  $(\sigma_v \delta_{v,v'} - \sigma_{vv'})$ .

#### 4.2.1 Gershgorin's circle theorem: proof that all the eigenvalues of the conductivity matrix are positive

Consider the matrix

$$M_{vv'} \equiv \sum_p m_p (\mathcal{A}_{vp} \delta_{vv'} - \mathcal{A}_{vp} \mathcal{A}_{v'p}),$$

where  $\mathcal{A}_{vp} \equiv \mathcal{A}(\mathbf{x}_v - \mathbf{x}_p)$ . From Gershgorin's circle theorem, we conclude the eigenvalues of  $M_{vv'}$  are always positive.

**Theorem 4.1.** Every eigenvalue,  $\lambda$ , of  $M_{vv'}$  lies in at least one of the circles  $C_1, \dots, C_n$ , where  $C_v$  has its center at the diagonal entry  $M_{vv}$  and its radius

$$R_v = \sum_{v \neq v'} |M_{vv'}|$$

equal to the absolute sum along the rest of the row [34, p. 426]. That is:

$$|\lambda - M_{vv}| \leq R_v. \tag{4.7}$$

First, we note that  $\mathcal{A}_{vp} \geq 0$  for all  $v$ , and that  $\sum_v \mathcal{A}_{vp} = 1$ . Thus,

$$R_v = \sum_{v \neq v'} \mathcal{A}_{vp} \mathcal{A}_{v'p} = \mathcal{A}_{vp} (1 - \mathcal{A}_{vp}) = M_{vv}. \tag{4.8}$$

Therefore,  $\lambda \geq 0$ . From this, we conclude that the error introduced by the substitution of the lumped conductivity is always dissipative.

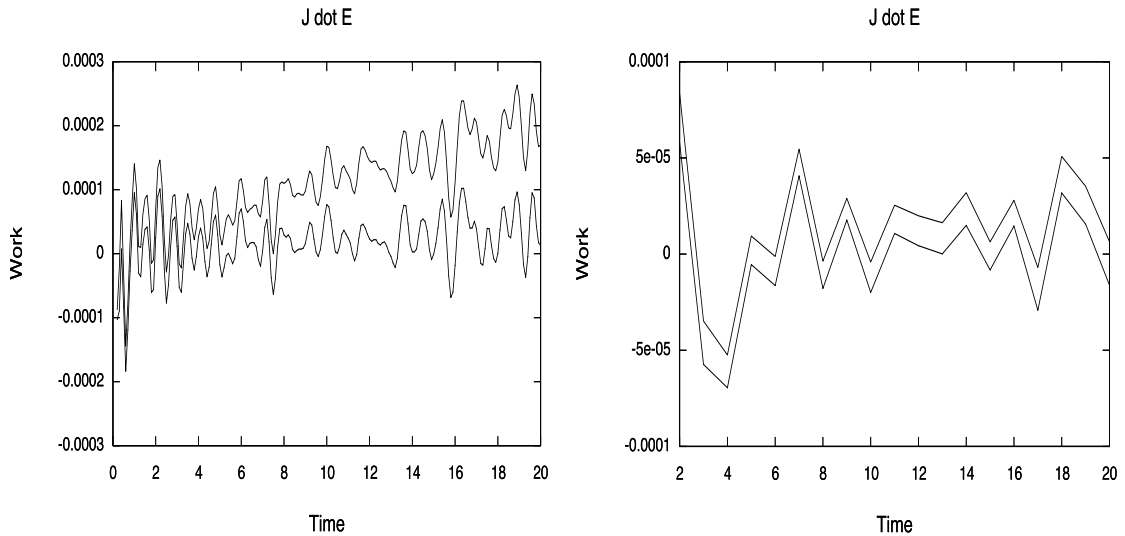


Figure 4: Work,  $\mathbf{J} \cdot \mathbf{E}$ , is shown for a short calculation with  $\omega_{pi}\Delta t = 0.1$  (left), and  $\omega_{pi}\Delta t = 1.0$  (right). The top curve in each plot is the work done by the fields, Eq. (2.13) and the bottom the work done on the particles, Eq. (2.14). Note that the work done on the particles is, on average, nearly zero for both cases. The difference between field and particle work is always positive for both time steps in agreement with Eq. (4.6), and corresponds to dissipation. The increase of dissipation with time, i.e. the difference, corresponds to the increase in the stochastic field with time.

In Fig. 4, we compare the work done by the fields with the work done on the particles. The problem is the same as the problem shown in Fig. 1. In the upper plot, the time step is  $\omega_{pi}\Delta t = 0.1$ , and in the lower plot,  $\omega_{pi}\Delta t = 1.0$ . For both time steps, the work done by the fields (upper curve) is always greater than the work done on the particles (lower curve), consistent with the proof above. In both cases, however, the total or time-integrated work done on the particles is small. The significance of the positive difference is that the error

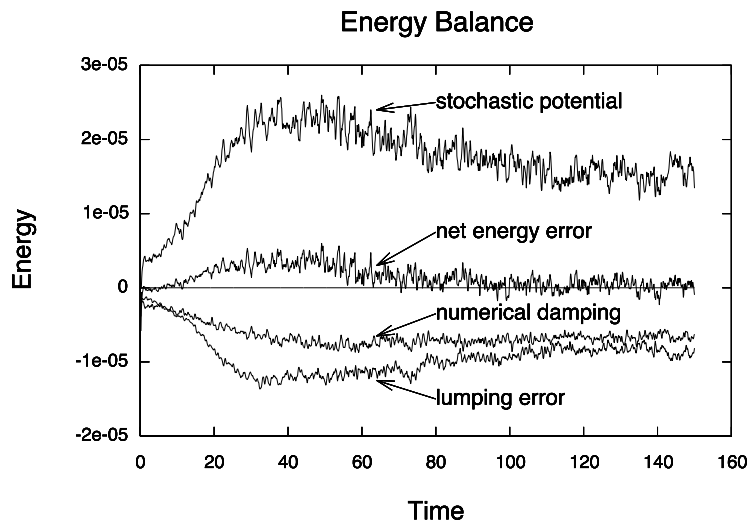


Figure 5: This figure summarizes the energy analysis. Stochastic heating, defined by Eq. (4.1), is balanced by the combined contributions of numerical damping, Eq. (2.13), and lumping error, Eq. (4.6). The net error is relatively small.

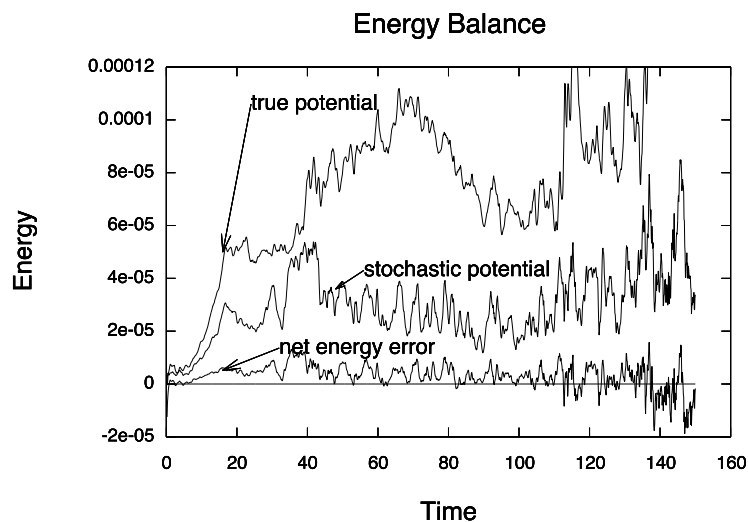


Figure 6: The electric field energy contributed by its scalar potential component (true potential energy), is larger than the stochastic potential energy, and much larger than the net energy error.

is always dissipative, and always tends to decrease total energy. A similar error occurs in fluid particle-in-cell codes. There, the lost energy is added to the internal energy of the particles to give conservation of total energy [6].

Fig. 5 shows how a balance between stochastic heating and numerical dissipation is achieved in the implicit calculations. The stochastic heating is balanced by the combined contributions of numerical damping, a time step dependent error, and 'lumping', a space

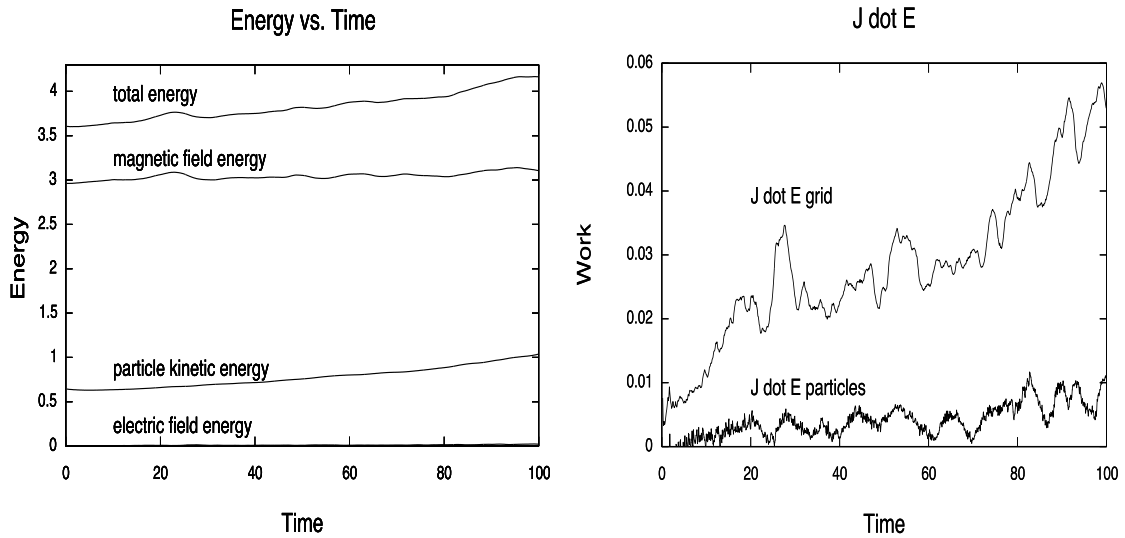


Figure 7: With  $u_e \Delta t / h$  as above, but a larger  $\omega_{pi}$ , a more MHD-like problem is solved. The particle energy nearly doubles in this short calculation (left). Although numerical damping nearly balances the heating due to the stochastic field, the work done on the particles is always positive (right). The upper curve is  $\mathbf{J} \cdot \mathbf{E}$  on the grid, Eq. (2.13), and the lower curve is the rate of change in particle energy, Eq. (2.15).

step dependent error. The net energy error is small, but not zero. The maximum of the net energy gain coincides roughly with the time at which the lower hybrid drift instability saturates. Fig. 6 compares the real and stochastic potentials. The 'real' potential is the scalar potential part of the electric field, and, and combines the 'stochastic' and lower-frequency potentials. The stochastic potential accounts for about a third of the total potential, but the net energy error is a very much smaller fraction of the real potential.

#### 4.2.2 MHD

We will consider two definitions of MHD. The first, in the sense used by Lapenta *et al.* in [23], is defined by quasi-neutrality and non-relativistic flow. This is approached with a large ion/electron mass ratio, but resolves the ion collisionless skin depth. A second definition observes the absence of length scales in MHD, and thus is approached as the ion gyroradius becomes small compared with the domain size. The Harris sheet equilibrium above approaches the MHD limit in this sense as the plasma density and field are increased without any change to  $h$  or  $\Delta t$ , if the ratios  $|\mathbf{B}|/n^{1/2}$  and  $|\mathbf{J}|/|\mathbf{B}|$  are constant. The current sheet thickness remains the same, and ratios, such as  $\omega_{ce}/\omega_{pe}$ , which characterize the problem are unchanged. In Fig. 7, we show the results for a calculation with  $100 \times$  the density of the problem shown in Fig. 1. For this calculation,  $\omega_{pi} \Delta t = 1.0$ . In the upper plot in Fig. 7, the heating is comparable to the earlier problem in  $1/10$  the time. In the lower plot, the upper curve is  $\mathbf{J} \cdot \mathbf{E}$  computed in on the grid, and the lower curve is the  $\mathbf{J} \cdot \mathbf{E}$  for the particles. The difference between grid and particle work terms is always positive, and this difference, the lumping error, decreases the total energy. Nevertheless,

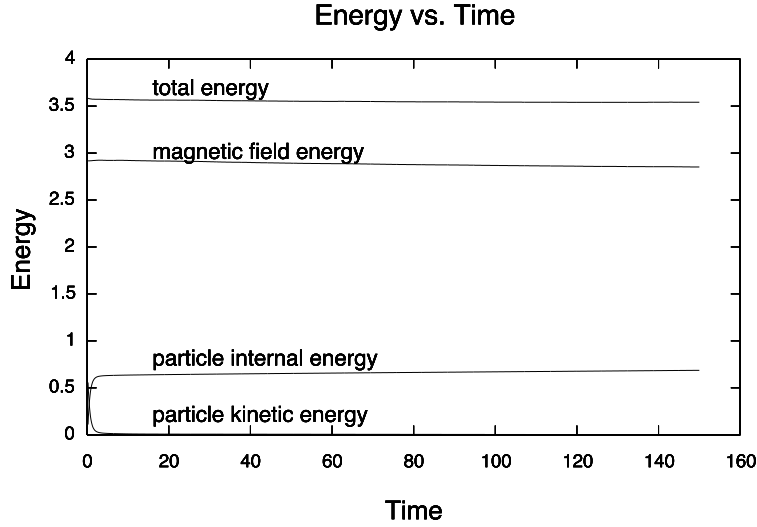


Figure 8: The problem of Fig. 7 is repeated with a collision frequency,  $\nu\Delta t = 0.1$ . The thermal energy of the particles is rapidly converted to internal energy. The magnetic field energy decreases slowly due to the momentum diffusion caused by lumping the mass matrix, Eq. (4.10). This causes a slow rise in the internal energy with time.

the total energy still increases at an unacceptable rate.

When collisions are added with  $\nu_e\Delta t = 1$ , the heating by stochastic fields is reduced, because the electron thermal energy is quickly converted to 'internal' energy, and the charge fluctuation amplitude approaches zero. In Fig. 8 with  $\nu_e\Delta t = \nu_i\Delta t = 1$ , the kinetic energy of the particles is quickly converted to internal energy, and there follows a slow decrease in magnetic energy and increase in particle internal energy. The total energy decreases slightly. This can be compared with the correct result, which is no change at all. Why is the solution not steady in time as expected?

One potential cause can be explored by considering the particle equation, Eq. (2.5), for  $\nu_s\Delta t \ll 1$ . For a high collision rate, the particle equation reduces to,

$$\mathbf{u}_p^{n+1} - \mathbf{u}_p^n \approx \nu_s \tau_s (\mathbf{u}_p^n - \mathbf{U}(\mathbf{x}_p)), \quad (4.9)$$

where  $\mathbf{U}(\mathbf{x}_p) = \sum_v \mathbf{U}_v \mathcal{A}_{vp}$ . (The center of mass velocity is calculated in the same way as the charge and current, Eq. (2.10)). The total particle momentum is a constant of the motion, but the center of mass velocity is not,

$$\begin{aligned} M_v (\mathbf{U}_v^{n+1} - \mathbf{U}_v^n) &= \sum_p m_p (\mathbf{u}_p^{n+1} - \mathbf{u}_p^n) \mathcal{A}_{vp}, \\ &= -\nu_s \tau_s \left[ \sum_p m_p \mathbf{u}_p^n \mathcal{A}_{vp} - \sum_{v'} \mathbf{U}_{v'} \sum_p m_p \mathcal{A}_{v'p} \mathcal{A}_{vp} \right] = -\sum_{v'} (M_v \delta_{vv'} - M_{vv'}) \mathbf{U}_{v'}^n. \end{aligned} \quad (4.10)$$

The mass matrix,  $M_{vv'}$ , is defined implicitly by Eq. (4.10), and results in an expression of the same form as discussed in Section 4.2. Clearly, the center of mass velocity is not

constant unless  $U_v = \text{const}$ , even though, globally, momentum is conserved. In the case of the current sheet equilibrium, the drift velocities slowly change. If the parameters were the same as for the reference case, the growth of the lower hybrid drift instability will cause shear flow to develop with time [21]. However, any process that causes inhomogeneities to develop in the density or flow velocity will cause the equilibrium to evolve. The observed energy decrease, seems like the correct result since the errors are diffusive in nature.

### 4.3 Solving the field equation

#### 4.3.1 Non-relativistic, quasi-neutral plasma, or how difficult is it to solve Eq. (3.29)

We consider a non-relativistic plasma,  $u_e/c \sim \epsilon < 1$ , which we wish to model on the ion time scale,  $\omega_{pi}\Delta t \sim 1.0$ . We ask what length scale do we resolve, and what is the relative size of the terms in the field equation.

The accuracy condition in the moment expansion,  $u_e\Delta t/h \sim \epsilon < 1$  constrains the ratio of  $\Delta t$  to the minimum resolved length scale,  $h$ . The time step we have chosen means that

$$\omega_{pe}\Delta t \sim (m_i/m_e)^{1/2}.$$

Thus, resolution of the ion collisionless skin depth is consistent with the accuracy condition,  $(c/\omega_{pi})/h \sim 1$ .

We now estimate the relative size of terms in the field equation Eq. (3.29). We scale the gradients by  $h$ ,  $h\nabla = \nabla'$ , drop numerical coefficients of order unity, and consider an unmagnetized plasma for which

$$4\pi\Delta t\sigma \approx (\omega_{pe}\Delta t)^2.$$

Combining the accuracy condition and the ratio  $u_e/c$ , we infer that  $c\Delta t/h \sim 1$ , and that a scaled Eq. (3.29) can be written,

$$\left(\frac{m_e}{m_i}\right)\nabla' \times \nabla' \times \mathbf{E}^{n+\theta} + \left(1 + \frac{m_e}{m_i}\right)\mathbf{E}^{n+\theta} \sim \left(\frac{m_e}{m_i}\right) \left[ \mathbf{E}^n + \nabla' \times \mathbf{B}^n - \frac{4\pi}{c} \hat{\mathbf{j}}h \right]. \quad (4.11)$$

The RHS is data, and thus arbitrary. The coefficients of the terms on the LHS give their relative magnitudes. Clearly, the solution of Eq. (4.11) approaches quasi-neutrality as the electron/ion mass ratio approaches its physical value, and

$$\lim_{m_e/m_i \rightarrow 0} \mathbf{E}^{n+\theta} = 0.$$

We also remark that the field equation, Eq. (3.29), is easy to solve on ion scales. A finite difference or finite element approximation to this equation will have a matrix representation with strong diagonal dominance. That is, numerically Eq. (3.29) becomes an algebraic equation for the electric field to lowest order. The differential operator is a perturbation.

### 4.3.2 Charge conservation

Solutions of the field equation, Eq. (3.29), must also satisfy Poisson's equation,

$$\nabla \cdot \left[ (\mathbf{I} + (\theta \Delta t) 4\pi\sigma) \cdot \mathbf{E}^{n+\theta} - \mathbf{E}^n + 4\pi\theta \Delta t \hat{\mathbf{j}} \right] = 0. \quad (4.12)$$

In both implicit moment and direct implicit methods, Poisson's equation is solved in addition to the field equation [5,20], because solutions of Eq. (3.29) don't satisfy Poisson's equation. Hewett and Langdon argue the cause is imperfect information in the solution of the field equation, which can be remedied by an adjustment of the longitudinal field [20]. While it is true that the errors are in charge accumulation, the difficulty is that the tensor conductivity in Eq. (4.12) couples the longitudinal and transverse electric fields, and a change in charge affects both [30].

Aside from correctness, the solution of Eq. (4.12) presents a challenge. Finding a more accurate and reliable algorithm for its solution is the theme of a series of papers over many years, among them a reformulation of Eq. (4.12) as a converging sequence of potential problems [1], and a multigrid-preconditioned Krylov method [17].

Mayergoyz argues that Maxwell's equations have more equations than boundary conditions as commonly solved, and remedies the deficiency by imposing additional boundary conditions [27]. Jiang *et al.* use their div-curl method to argue that if one solves a partial differential equation on the boundary to compute boundary conditions for the field equation, Eq. (3.29), Poisson's equation will also be solved [15]. Ricci *et al.* applied this method to implicit simulation, and satisfied Poisson's equation to an accuracy determined by the truncation error of the boundary equations without the need to solve Poisson's equation in the volume [30].

Subsequent work on this problem, which is outlined in [8], eliminates the need to solve a partial differential equation on the boundary. One assumes that the vector  $\mathbf{E}$  solves Eq. (3.29), and thus that inner product of this equation with a suitable test vector  $\mathbf{E}'$  is zero. But, by the Helmholtz decomposition theorem,  $\mathbf{E}'$  can be decomposed into divergence-free and curl-free parts,

$$\mathbf{E}' = -\nabla\phi + \mathbf{A},$$

where  $\nabla \cdot \mathbf{A} = 0$ . The inner product of  $\nabla\phi$  with (3.29) is of course zero. If it is integrated by parts the surface contributions are zero when the following boundary conditions are satisfied: On magnetic symmetry boundaries where  $\hat{\mathbf{n}} \times \nabla \times \mathbf{E} = 0$  it is necessary that,

$$\hat{\mathbf{n}} \cdot \left[ (\mathbf{I} + (\theta \Delta t) 4\pi\sigma) \cdot \mathbf{E}^{n+\theta} - \mathbf{E}^n + 4\pi\theta \Delta t \hat{\mathbf{j}} \right] = 0. \quad (4.13)$$

On conducting boundaries where  $\hat{\mathbf{n}} \times \mathbf{E} = 0$ , a compatibility condition must be satisfied,

$$\int_{\partial D} \hat{\mathbf{n}} \cdot \left[ (\mathbf{I} + (\theta \Delta t) 4\pi\sigma) \cdot \mathbf{E}^{n+\theta} - \mathbf{E}^n + 4\pi\theta \Delta t \hat{\mathbf{j}} \right] d\mathbf{S} = 0. \quad (4.14)$$

Since the surface contributions are zero because of the boundary conditions, the volume contribution must also be zero,

$$\int_D \phi \left[ \nabla \cdot \left[ (\mathbf{I} + (\theta \Delta t) 4\pi \sigma) \cdot \mathbf{E}^{n+\theta} - \mathbf{E}^n + 4\pi \theta \Delta t \hat{\mathbf{j}} \right] \right] dV = 0, \tag{4.15}$$

for arbitrary  $\phi$ .

This proof depends upon the vector identity,

$$\nabla \cdot \nabla \times \mathbf{V} = 0,$$

where  $\mathbf{V}$  is an arbitrary vector. We now show that the geometric coefficients preserve this identity on a regular rectilinear grid, and the proof is valid for the difference equations.

First, consider Eq. (2.3), the solenoidal condition for the magnetic field. Using generalized geometric coefficients, the approximation to  $\nabla \cdot \partial \mathbf{B} / \partial t$  is,

$$-\sum_c \mathbf{g}_{cv} \cdot \frac{1}{V_c} \sum_{v'} \mathbf{g}_{cv'} \times \mathbf{E}_{v'} = -\sum_c \mathbf{g}_{cv} \cdot \frac{\mathbf{B}_c^{n+1} - \mathbf{B}_c^n}{c \Delta t}. \tag{4.16}$$

Interchange the order of summation and use a vector identity to interchange vector operations, and get,

$$-\sum_c \mathbf{g}_{cv} \cdot \frac{1}{V_c} \sum_{v'} \mathbf{g}_{cv'} \times \mathbf{E}'_{v'} = -\sum_{v'} \sum_c \frac{(\mathbf{g}_{cv} \times \mathbf{g}_{cv'})}{V_c} \cdot \mathbf{E}_{v'}. \tag{4.17}$$

On a rectilinear mesh with constant spacing, the geometric coefficients are the same in all cells, and sum over  $c$  on the RHS. The result is that it equals the negative of itself,

$$\sum_c (\mathbf{g}_{cv} \times \mathbf{g}_{cv'}) = \sum_c (\mathbf{g}_{cv'} \times \mathbf{g}_{cv}), \tag{4.18}$$

and therefore must be zero. Thus, if  $\nabla \cdot \mathbf{B} = 0$  initially, it will always equal zero.

The same method of proof shows that the numerical divergence operator acting on Eq. (3.29) yields Poisson's equation, Eq. (4.12) on a regular, rectilinear mesh.

In the solutions discussed in Section (4.1), both the field equation and Poisson's equation are satisfied to the same accuracy,  $error < 10^{-10}$ .

## 5 Remarks

The elimination of the need to solve Eq. (4.12) as a separate step simplifies the field solution substantially. The work in [31] eliminates the equation in the volume, and [8] eliminates the equation on the boundary and yields more accurate solutions. The scaling of the field equation, Eq. (3.29), suggests that it will be no more difficult to solve in the quasi-neutral limit, but numerical experiments indicate that some preconditioning of the Krylov solver might increase efficiency.

Our analysis shows how stochastic heating has been managed in implicit kinetic calculations. When it is not possible to reduce heating by increasing the number of particles, the negative-definite errors in energy contributed by using a lumped conductivity matrix and a  $\theta > 1/2$  time centering in the implicit equations may still be sufficient to control heating when

$$u_e \Delta t / h \ll 1.$$

That the accuracy condition in the moment expansion and the condition for a balancing of dissipation and stochastic heating should be the same seems a happy outcome, but is it accidental? In [3], it is argued that dissipation due to using  $\theta > 1/2$  dissipates frequencies near the Nyquist time frequency most efficiently. Similarly, the error from using a lumped conductivity matrix is largest at short wavelengths. The error can be estimated for an area-weighting assignment function using its Fourier transform,

$$\mathcal{A}_k = (\sin(kh/2)/(kh/2))^2,$$

where  $k$  is the wave number. The ratio of the estimated error, Eq. (4.6), to  $\mathbf{J} \cdot \mathbf{E}$  evaluated at the spatial Nyquist frequency,

$$kh = \pi,$$

is nearly 90%. Thus, spatial frequencies near the Nyquist space frequency are strongly damped. On the other hand, statistical fluctuations in the charge density decrease with sample size, so that the stochastic fields they produce should be concentrated at high frequencies and short wavelengths. Finally, the accuracy condition causes the scaling of the dissipation and the stochastic field amplitude to be linked.

If one attempts to solve a problem on an MHD time scale, the strategies above no longer suffice. For these problems, the heating rate is substantially higher. Stochastic heating is eliminated by collisions, but at the cost of suppressing kinetic phenomena. However, for the kind of problems described in [33], where one combines fluid and kinetic calculations to accommodate wide variations in time and length scales, a method which uses the same equations and solvers everywhere and only changes the collision frequency to move from kinetic to fluid models, has many advantages. That is, a change in grid size, time step, and collision frequency will distinguish regions where detailed kinetic simulations are underway from regions where a plasma in local thermodynamic equilibrium is undergoing large-scale, quasi-neutral flow. There may ultimately be roadblocks preventing realization of this ultimate goal, but the efforts toward it have already yielded the improvements in simulation technology outlined in this paper.

Finally, we remark that both the form of the collision model and the value of the constant collision frequency are unphysical. However, they provide a means to test the fluid limit of the kinetic equations, and their introduction results in solutions of multifluid, magnetohydrodynamic equations with electron inertia retained. More physical collision models and collision frequencies will surely reduce stochastic heating less, simply because they will be less effective at converting particle kinetic energy into internal energy.

## Acknowledgments

This material is based upon work supported by the National Science Foundation under Grant No. 0614006. Many useful discussions with Paolo Ricci are gratefully acknowledged.

## References

- [1] P. A. Bernhardt and J. U. Brackbill, Solution of elliptic equations using fast Poisson solvers, *J. Comput. Phys.* **53**(1984) 382.
- [2] J. U. Brackbill, Numerical magnetohydrodynamics for high-beta plasmas, *Meth. in Comput. Phys.* **16**(1976) 141.
- [3] J. U. Brackbill and D. W. Forslund, An implicit method for electromagnetic plasma simulation in two dimensions, *J. Comput. Phys.* **46** (1982)271.
- [4] J. U. Brackbill, D. W. Forslund, K. B. Quest and D. Winske, Nonlinear evolution of the lower hybrid drift instability, *Phys. Fluids*, **27** (1984) 2682.
- [5] J. U. Brackbill and D. W. Forslund, Simulation of low-frequency. electromagnetic phenomena in plasmas, pp271-310 in 'Multiple Times Scales', J. U. Brackbill and B. I. Cohen, eds, Academic Press, NY, 1986.
- [6] J. U. Brackbill and H. M. Ruppel, FLIP: A method for adaptively zoned, particle-in-cell calculations of fluid flows in two dimensions, *J. Comput. Phys.* **65**(1986) 314.
- [7] J. U. Brackbill, Numerical methods for charged particle transport: Particle-in-cell methods, Proceedings of the Premier Ecole d'Ete, J. C. Adam editor, GdR SPARCH, Oleron, France, September 1993.
- [8] J. U. Brackbill, Boundary conditions for Maxwell solvers, *J. Comput. Phys.* **227** (2008), 6715-6719.
- [9] B. I. Cohen, A. Bruce Langdon and D. W. Hewett, Performance and optimization of direct implicit particle simulation, *J. Comput. Phys.* **81** (1989), 151-168.
- [10] D. W. Forslund and J. U. Brackbill, Magnetic field enhanced lateral transport in laser irradiated plasmas, *Phys. Rev. Lett.* **48**(1982) 1614.
- [11] D. W. Forslund, K. B. Quest, J. U. Brackbill and K. Lee, Collisionless dissipation in quasi-perpendicular shocks, *J. Geophys. Res.* **89** (1984) 2142-2150.
- [12] D. A. Knoll, G. Lapenta and J. U. Brackbill, A multilevel iterative field solver for implicit, kinetic plasma simulation, *J. Comput. Phys.* **149** (1999) 377-388.
- [13] J. Denavit, Time-filtering particle simulations with  $\omega_{pe}\Delta t \ll 1$ , *J. Comput. Phys.* **42**(1981) 337-366.
- [14] R. R. Hockney, Measurements of collision and heating times in a two-dimensional thermal computer plasma, *J. Comput. Phys.* **8**(1971) 19-44.
- [15] B.-N. Jiang, J. Wu and L. A. Povinelli, The origin of spurious solutions in computational electromagnetics, *J. Comput. Phys.* **125** (1996) 104-123.
- [16] T. Kamimura, E. Montalvo, D. C. Barnes, J. N. Leboeuf and T. Tajima, Implicit particle simulation of electromagnetic plasma phenomena, *J. Comput. Phys.* **100**(1992) 77-90.
- [17] D. A. Knoll, G. Lapenta and J. U. Brackbill, A multilevel iterative field solver for implicit, kinetic plasma simulation, *J. Comput. Phys.* **140**(1999) 377-388.
- [18] A. Bruce Langdon, Effects of the spatial grid in simulation plasmas, *J. Comput. Phys.* **6** (1970) 247-267.

- [19] A. Bruce Langdon, B. I. Cohen and A. Friedman, Direct implicit large time-step particle simulation of plasmas, *J. Comput. Phys.* **51** (1983) 107-138.
- [20] D. W. Hewett and A. Bruce Langdon, Electromagnetic direct implicit plasma simulation, *J. Comput. Phys.* **72** (1987) 121-155.
- [21] G. Lapenta and J. U. Brackbill, Nonlinear evolution of the lower hybrid drift instability: Current sheet thinning and kinking, *Phys. Plasmas* **9** (2002) 1544.
- [22] G. Lapenta, J. U. Brackbill and W. S. Daughton, The unexpected role of the lower hybrid drift instability in magnetic reconnection in three dimensions, *Phys. Plasmas* **10**(2003)1577-1587.
- [23] G. Lapenta, J. U. Brackbill and P. Ricci, Kinetic approach to microscopic-macroscopic coupling in space and laboratory plasmas, *Phys. Plasmas*, **13**(2006)055904.
- [24] E. L. Lindman, Dispersion relation for computer-simulated plasmas, *J. Comput. Phys.* **5** (1970) 13-22.
- [25] R. J. Mason, Implicit moment particle simulation of plasmas, *J. Comput. Phys.* **41** (1981) 233-244.
- [26] R. J. Mason, Hybrid and collisional implicit plasma simulation models, pp233-270 in 'Multiple Times Scales', J. U. Brackbill and B. I. Cohen, eds, Academic Press, NY, 1986.
- [27] I. D. Mayergoyz and J. D'Angelo, A new point of view on the mathematical structure of Maxwell's equations, *IEEE Transactions on Magnetics*, **29**(1993) 1315-1320.
- [28] K. B. Quest, D. W. Forslund, J. U. Brackbill and K. Lee, Collisionless dissipation in quasi-parallel shocks, *Geophys. Res. Lett* **10** (1983) 471-474.
- [29] A. D. Richmond, Ionospheric electrodynamics using magnetic apex coordinates, *J. Geomag. Geoelectr.* **47** (1995) 191-212.
- [30] P. Ricci, G. Lapenta and J. U. Brackbill, A simplified implicit Maxwell solver, *J. Comput. Phys.* **183** (2001) 117-141.
- [31] P. Ricci, J. U. Brackbill, W. Daughton and G. Lapenta, Influence of the lower hybrid drift instability on the onset of magnetic reconnection, *Phys. Plasmas* **11** (2004) 4489.
- [32] W. D. Schulz, Two-dimensional Lagrangian hydrodynamic difference equations, *Meth. in Comput. Phys.* **3**(1964)1-45.
- [33] T. Sugiyama and K. Kusano, Multi-scale plasma simulation by the interlocking of magnetohydrodynamic model and particle-in-cell code, *J. Comput. Phys.* (2007), doi:10.1016/j.jcp.2007.09.011.
- [34] G. Strang, "Introduction to Applied Mathematics", Wellesley-Cambridge Press, Cambridge, MA, 1986.
- [35] M. Tanaka, The macro-EM particle simulation method and a study of collisionless magnetic reconnection, *Comput. Phys. Commun.* **87**(1995) 117-138.
- [36] M. A. Yates, D. B. v. Hulsteyn, H. Rutkowski, G. Kyrala and J. U. Brackbill, Experimental evidence for self-generated magnetic fields and remote energy deposition in laser irradiated targets, *Phys. Rev. Lett.* **49** 1982, 1702.